DOI: 10.11835/j.issn.2096-6717.2026.038

开放科学(资源服务)标识码OSID:

崩塌涌浪数值模拟中的参数敏感性与不确定性分析

原辉[1],芦竹茂[1],徐思卿[1],张伟[2],卢望[3]

(1.国网山西省电力公司电力科学研究院,太原 030013;2.国网山西省电力有限公司,太原 030013;3.重庆大学 土木工程学院,重庆 400045)

摘　要:滑坡涌浪是水库库区一种典型的次生灾害。当前的风险评估往往侧重于极端水位情况,且对关键的滑坡运动参数采用确定性的数值,这可能会导致对灾害风险的理解不全面。为了揭示位于中国重庆的箭穿洞危岩在代表性正常水位下崩塌诱发涌浪的特征,并量化涌浪预测对恢复系数(COR)和摩擦系数(COF)的敏感性,采用FLOW-3D软件建立三维流固耦合数值模型,其中危岩体采用广义运动物体模拟,并用FAVOR方法追踪界面,模拟了162 m水位下的涌浪过程,并通过将COR与COF增减±20%进行单因素敏感性分析。结果表明,崩塌产生的涌浪最大波幅为27.4 m,其演化经历了明显的生成、传播、爬高和消散阶段。敏感性分析结果表明,COF主导控制着最低自由液面高程(变化-20%时,相对敏感系数RSC约为-1.27),而COR主要控制着岩体的最大运动速度(变化-20%时,RSC约为-0.52)。相比之下,最大波高对这些参数变化极不敏感。涌浪灾害评估必须考虑有代表性的水库运行水位以及关键不确定参数对不同评价指标不对称、有选择的敏感性。

关键词:水库;涌浪;岩壁崩塌;灾害评估;数值模拟

中图分类号:TV139.2　　**文献标志码:**A　　**文章编号:**2096-6717(XXXX)XX-0001-12

Parameter sensitivity and uncertainty analysis in the numerical simulation of landslide-generated impulse waves

YUAN Hui[1], *LU Zhumao*[1], *XU Siqing*[1], *ZHANG Wei*[2], *LU Wang*[3]

(1. State Grid Shanxi Electric Power Co., LTD. Research Institute, Taiyuan 030013, P. R. China; 2. State Grid Shanxi Electric Power Co., LTD., Taiyuan 030013, P. R. China; 3. School of Civil Engineering, Chongqing University, Chongqing 400045, P. R. China)

Abstract: Landslide-generated impulse waves pose a significant secondary hazard in reservoir areas. Current risk assessments often prioritize extreme water levels and rely on deterministic values for key landslide kinematic parameters, which may lead to an incomplete understanding of the full hazard spectrum. This study aimed to investigate the characteristics of impulse waves from the potential collapse of the Jianchuandong rocky cliff (Chongqing City, China) under a representative normal water level, and to quantify the sensitivity of wave predictions to the coefficient of restitution (COR) and coefficient of friction (COF). A three-dimensional fluid-solid coupling numerical model was established using FLOW-3D software. The simulation incorporated a general moving object for the rock mass and the fractional area/volume obstacle representation method for interface tracking. The impulse wave process under a 162 m water level was simulated, and a one-at-a-time

Received: 2026-03-03

Foundation items: The Science and Technology Foundation of State Grid Corporation of China (No. 5200-202415102A-1-1-ZN)

Author brief: YUAN Hui (1988-), senior engineer, main research interest: meteorological disaster, E-mail: yuanhuidky@163.com.

sensitivity analysis was performed by varying the COR and COF by ± 20%. The results showed that the collapse generated an impulse wave with a maximum amplitude of 27.4 m, evolving through distinct generation, propagation, run-up, and dissipation phases. The sensitivity analysis revealed that the COF dominantly controlled the minimum free surface elevation (relative sensitivity coefficient, RSC, approximately - 1.27 for a - 20% change), whereas the COR primarily governed the maximum rock mass velocity (RSC approximately - 0.52 for a - 20% change). In contrast, the maximum wave height was notably insensitive to these parameter variations. This study concludes that wave hazard assessments must account for the representative operational water levels and the asymmetric, metric-specific sensitivities of key uncertain parameters.

Keywords: reservoir; impulse waves; rocky cliff collapse; hazard assessment; numerical simulation

1 Introduction

Landslide-generated impulse waves triggered by reservoir bank instability represent a severe secondary hazard for large-scale water conservancy projects. When a massive volume of rock and soil impacts a water body at high velocity, intense fluid-solid coupling interactions instantaneously convert the gravitational potential energy of the landslide mass into the kinetic energy of the water, generating highly destructive giant waves[1]. This phenomenon not only seriously threatens the lives, property, and safety of residents along the reservoir shores but can also inflict catastrophic damage to dams and navigation facilities. China's Three Gorges Reservoir (TGR) is the world's largest hydroelectric project and is situated in a geologically complex area hosting numerous high-position unstable rock masses. Since its impoundment in 2003, several significant landslide-generated wave events have occurred within the reservoir area, such as the Qianjiangping landslide in 2003 and the Gongjiafang landslide in 2008, both of which caused substantial societal impact and economic losses[2-4]. Therefore, conducting in-depth studies on the generation and propagation mechanisms of impulse waves from typical unstable rock masses is of significant practical importance. Such studies are essential for enhancing comprehensive disaster prevention and mitigation capabilities in reservoir areas[5-6].

The generation of landslide-induced waves is a complex dynamic process involving solid-liquid-gas three-phase coupling, governed by multiple factors including the kinematic characteristics of the slide mass, geometry of the water body, and hydrodynamic conditions. Early studies primarily relied on physical model tests and empirical formulas, that although intuitive, were limited by scale effects and high costs[7-8]. With the rapid advancement of computational fluid dynamics (CFD) technology, numerical simulation has become the predominant method for studying landslide-generated waves[9-11]. Numerical models based on the Reynolds-averaged Navier-Stokes (RANS) equations combined with the volume of fluid (VOF) method are particularly noteworthy. Their capability to accurately capture free surface deformation and multi-phase flow interactions has led to their widespread application in wave hazard assessment[12-13]. For more coherent rock avalanches, coupling rigid body motion models (e. g., the general moving object (GMO) model in FLOW-3D) with fluid equations have significantly improved computational efficiency while maintaining physical realism, enabling detailed simulations under multiple scenarios[14]. However, a review of simulation studies on wave hazards in the TGR area (e. g., targeting the Jianchuandong unstable rock mass) reveals two significant limitations that constrain a comprehensive understanding of the disaster risk.

First, studies have predominantly focused on two extreme operational water levels: the minimum (145 m) and the maximum design levels (175 m)[15]. While it is true that the 145 m level may lead to the maximum initial wave height due to the greatest fall height, and the 175 m level may pose the greatest run-up threat due to the highest base elevation, the actual operational scheduling of the TGR involves dynamic adjustment of the water level between 145 m and 175 m. Based on the practical needs of reservoir sediment flushing and ecological scheduling, the

forebay water level often maintains a prolonged duration within the range of 160 m to 162 m during both impoundment and drawdown periods. This constitutes a normalized operational characteristic water level for the reservoir. Statistical analysis of TGR water level data by Huang et al. [16] indicates that the annual average water level at the Three Gorges Dam is approximately 162-163 m. Neglecting studies on this normal water level, which has a high probability of exposure, may create a blind spot in the lifecycle risk assessment of wave hazards and fail to accurately reflect the comprehensive risk level under long-term reservoir operation. Furthermore, accurately assessing the comprehensive wave hazard under this highly probable normal water level requires not only capturing the specific hydrodynamic boundaries but also addressing the inherent uncertainties within the sliding process itself.

Second, within numerical simulations, the kinematic parameters of the landslide mass have a decisive influence on the energy transfer during wave generation, with the coefficient of restitution (COR) and the coefficient of friction (COF) being particularly critical. The COF governs the entry velocity of the landslide, directly determining the magnitude of the Froude number, whereas the COR dictates the energy dissipation efficiency during the interaction between the rock mass and the slope surface[17-18]. However, constrained by geological survey uncertainties, studies often assign fixed empirical values to these parameters, lacking systematic sensitivity analyses. This deterministic approach masks the potentially significant perturbation of the parameter variability on wave prediction outcomes, limiting the applicability of the model and the robustness of its predictions in complex and variable geological environments.

Addressing the aforementioned gaps and aligning with the current academic frontier shifting from "simulation and reproduction" to "uncertainty quantification" in landslide wave research, this study focuses on the typical Jianchuandong unstable rock mass in the Wu Gorge section of the TGR. Using the FLOW-3D software, a three-dimensional fluid-solid coupling numerical model is established with the following two novel objectives: (1) to simulate and reveal the characteristics of impulse wave generation, propagation, and run-up triggered by rock mass collapse under the 162 m normal water level, thereby filling the gap between extreme level scenarios and refining the understanding of hazards across the entire water level cycle; (2) to conduct a parameter sensitivity analysis on the COR and COF, quantifying the influence weights of these key physical parameters on wave characteristics (wave height, flow velocity, and run-up) and elucidating the energy conversion and dissipation mechanisms from gravitational potential energy to water wave energy. The findings of this study will provide a scientific basis for the refined risk assessment and uncertainty management of landslide-generated impulse waves in the TGR area.

2 Methodology

2.1 Governing Equations

To address the strong non-linear fluid-solid coupling involved in rocky cliff collapses, this study establishes a three-dimensional numerical framework within the FLOW-3D platform. The hydrodynamic characteristics of the flow field are characterized by the RANS equations, which provide a robust solution for macro-scale flow simulations while maintaining physical rigor. To accurately capture the intense turbulent fluctuations and energy dissipation during wave generation, the model incorporates the RNG k-ϵ turbulence closure based on the re-normalization group theory. Compared to standard models, the RNG k-ϵ variant exhibits superior performance in handling complex flows with high-curvature streamlines and strong shear, significantly enhancing numerical stability and precision during wave breaking and near-shore evolution.

2.2 Free Surface and Complex Boundary Treatment

The tracking of the free surface and the treatment of complex boundaries are achieved through the integration of the VOF method and the fractional area/volume obstacle representation (FAVOR) technology. The VOF method tracks the fluid volume fraction within cells to adaptively capture topological changes in the wave front, such as curling, breaking, and air entrainment, without the need for complex mesh reconstruction. Simultaneously, FAVOR technology circumvents the limitations of body-fitted co-

ordinates by calculating the fractional area and volume of solid geometries within a structured Cartesian grid. This "free-gridding" approach not only streamlines pre-processing but also eliminates the numerical energy losses associated with "zigzag" approximations of curved boundaries, ensuring the fidelity of boundary layer flow calculations.

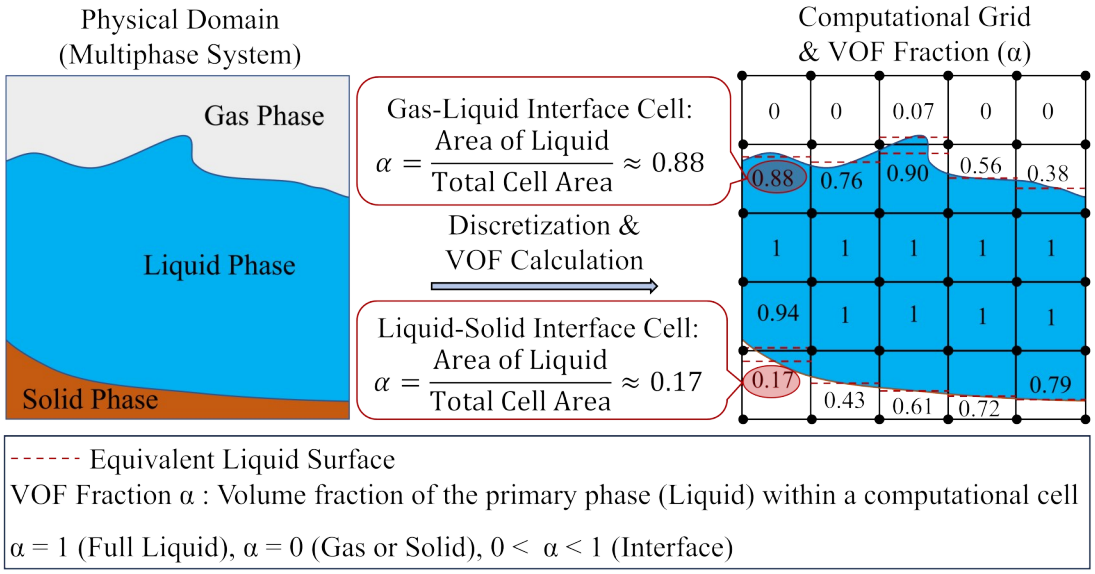

Fig. 1 Schematic diagram of the volume-fraction method (Adapted from Hirt[19])

2.3 Rock Mass Motion Model

The kinematic response of the rock mass is implemented via the GMO model, treating the unstable mass as a rigid body with six degrees of freedom. The GMO model uses a two-way coupling mechanism: the hydrodynamic pressure and shear stress exerted by the fluid determine the trajectory of the rock and entry velocity, whereas the instantaneous displacement and acceleration of the rock drive the surrounding water to generate the initial impulse. This algorithm ensures strict energy conservation between the solid and liquid phases, providing a solid technical foundation for simulating the entire process, from initial instability and accelerated sliding to high-speed impact and far-field wave propagation.

2.4 One-at-a-Time Sensitivity Analysis

One-at-a-time (OAT) sensitivity analysis is a local sensitivity method used to evaluate the influence of individual parameter variations on model outputs while keeping all other parameters fixed at their baseline values. This method systematically quantifies the independent effect of each input parameter.

Consider a model output y defined as a function f of a parameter vector $\boldsymbol{p} = (p_1, p_2, \cdots, p_n)$:

$$y = f(p) \tag{1}$$

Given a set of baseline parameter values $\mathrm{p}_0 = (p_1^0, p_2^0, \cdots, p_n^0)$, a single parameter p_i is varied by a relative perturbation δ_i (typically $\pm$ 10%, $\pm$ 20%), whereas all the other parameters remain constant:

$$p_i = p_i^0 \times (1 + \delta_i) \tag{2}$$

The corresponding change in the model output is:

$$\Delta y_i = f(p_1^0, \cdots, p_i, \cdots, p_n^0) - f(p_0) \tag{3}$$

To facilitate comparison across parameters with different units and magnitudes, a normalized metric, the relative sensitivity coefficient (RSC), is commonly calculated (see Equation 4):

$$S_i = \frac{\Delta y_i / y_0}{\Delta p_i / p_i^0} \tag{4}$$

Where $y_0 = f(\mathrm{p}_0)$ and $\Delta p_i = p_i - p_i^0$. A larger S_i absolute value indicates a greater influence of parameter p_i on the model output.

3 Analysis of Impulse Wave Simulation

3.1 Jianchuandong Rocky Cliff

The Jianchuandong unstable rock mass is located on the left bank of the Yangtze River in Wushan County, Chongqing Municipality, within the TGR area, China. It is situated approximately 15 km from

Wushan County town, at the slope toe on the western side of the famous Shennv Peak in the Wu Gorge. The site is about 1.3 km upstream from the downstream Qingshi Wharf and residential areas. Figure 2 illustrates the geographical location of the rock mass. Should instability occur at Jianchuandong, it would not only threaten navigation in the main channel of the Yangtze River but also generate impulse waves posing a risk to the nearby wharf and residential zones.

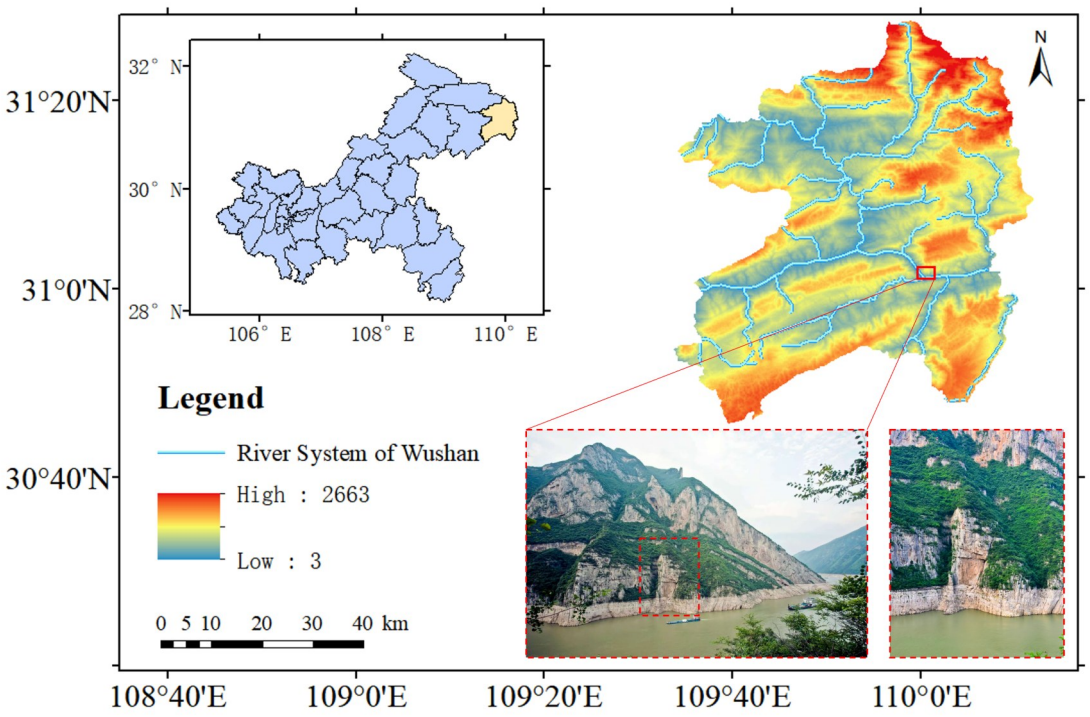

Fig. 2　Geographical location of the Jianchuandong unstable rock mass

The Jianchuandong rock mass is delineated by three major discontinuities, as shown in Figure 3. Discontinuity 1 is a tectonic transverse tension crack. Its aperture generally ranges from 1 to 70 cm, widening to 3.15 m at the rear unloading section. It is partially filled with rock fragments or debris, exhibits an uneven fracture surface, and has a spacing typically around 3.3 m (ranging from 2.2 to 4.9 m). Most segments extend over 50 m in length. The fracture surfaces exhibit poor cohesion, classifying it as a hard structural plane. Discontinuity 2 is a tectonic longitudinal tension crack. Its aperture mostly ranges from 1 to 20 cm, reaching 1.25 m at the upstream boundary. It is also largely partially filled with rock fragments or debris and has an uneven surface. The spacing is typically approximately 2.4 m (ranging from 1.7 to 4.1 m), with most segments extending over 50 m. Similarly, it features poor surface cohesion and is a hard structural plane. Discontinuity 3 at the rear scarp has a maximum aperture of 3.15 m. The lower portion of this crack below the 226 m elevation is filled with crushed rock.

The three-dimensional boundaries of the Jianchuandong unstable rock mass are well-defined. The rear scarp elevation ranges from 278 to 305 m, whereas the base elevation is 155 m, resulting in an average height difference of 135 m. The rock mass has an average width of approximately 55 m and an average thickness of about 50 m, yielding an estimated volume of 360 000 m^3.

The rock mass foundation consists of banded marlstone, whereas the overlying rock is dense limestone. Previous studies illustrate the detailed geological conditions of the Jianchuandong unstable rock mass[14-15]. The foundation rock has relatively lower strength. The splitting cracks observed in the foundation are likely compression-induced fractures resulting from the overlying load. As the unstable rock mass has largely separated from the parent rock, its weight acts directly on the foundation, causing the development of longitudinal tension cracks and shear fractures analogous to those under uniaxial compression. The failure of the foundation rock, in turn, can further promote the opening and propagation of the

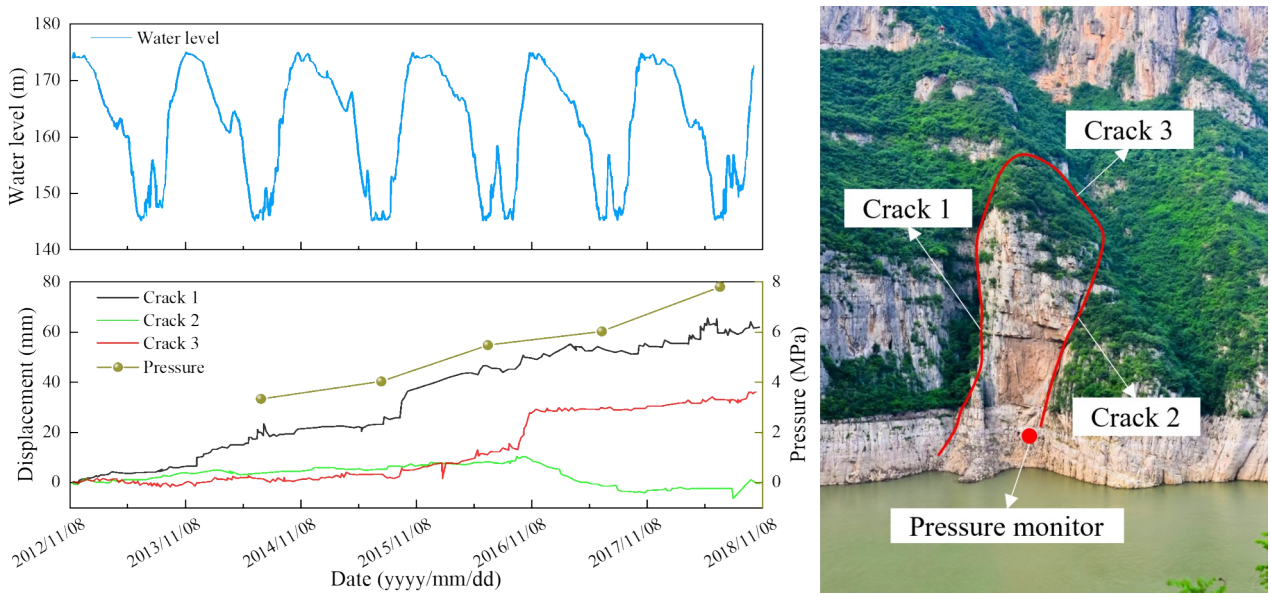

Fig. 3 Six-year monitoring data of displacement and pressure for the Jianchuandong unstable rock mass[20]

rear scarp crack, jeopardizing the overall stability of the rock mass. Moreover, with its top elevation at 155 m, the foundation lies within the water-level fluctuation zone of the TGR, between the low water level of 145 m and the high-water level of 175 m. Periodic water-level fluctuations and water-rock interaction in this zone can lead to the reduction of rock strength, potentially triggering instability.

Based on displacement monitoring data for the Jianchuandong unstable rock mass and pressure measurements at its foundation, the foundation pressure has been increasing. Concurrently, significant widening has been observed in the rear scarp crack and the left-side Discontinuity 1. Consequently, it can be inferred that during cyclic water-level changes, the foundation rock undergoes wet-dry cycles, leading to a gradual decrease in its strength. This degradation induces an overall failure tendency in the rock mass.

Combining detailed geological investigations with long-term monitoring data, the most probable failure mode of the Jianchuandong unstable rock mass is identified as toppling. The foundation of the rock mass consists of banded marlstone, which is relatively weak and situated precisely within the water-level fluctuation zone of the TGR. Periodic reservoir operations expose the foundation to cyclic wet-dry cycles, leading to progressive deterioration of the rock strength. This deterioration is particularly pronounced at the front edge of the foundation, which is in direct contact with the water and subjected to both chemical weathering and physical scouring. The combined effects result in the erosion and removal of the front foundation rock, gradually forming cavities. As the frontal support diminishes, the overlying dense limestone mass, already separated from the parent rock by rear cracks, tends to tilt forward under gravity. This toppling tendency is corroborated by monitoring data: the pressure on the foundation has been increasing, whereas the rear scarp crack and the left-side discontinuity (Discontinuity 1) have widened significantly.

These complex geological and environmental conditions directly govern the parameterization and inherent uncertainties within the subsequent numerical model. Specifically, the baseline of COF and COR used in the simulation was assigned to reflect the macroscopic frictional resistance of the debris-filled discontinuities and the heavily weathered banded marlstone foundation along the toppling and sliding path. However, the progressive and uneven degradation of the rock mass subjected to cyclic wet-dry conditions in the water-level fluctuation zone dictates that the sliding surface cannot maintain a uniform or constant shear strength. This spatiotemporal variability in geological conditions makes it impossible to rely on a single deterministic friction coefficient, fundamentally requiring the targeted parameter sensitivity analysis conducted in this study.

3.2 Modelling Process of Impulse Waves Generated by the Jianchuandong Rocky Cliff

A three-dimensional geological model of the Jianchuandong rocky cliff and the surrounding reservoir

area was established based on a high-precision digital elevation model (DEM) with a 5-m resolution. This model is used to simulate the impulse waves induced by the toppling failure of the Jianchuandong unstable rock mass into the water. The rock mass at the foundation of Jianchuandong is subjected to the cyclic fluctuation of reservoir water levels and undergoes progressive deterioration. Combined with the erosive and physical scouring effects of the reservoir water, the foundation rock is likely to fail first, which may subsequently trigger the overall topple and collapse of the unstable rock mass.

The viscous flow model was selected for the simulation, with the re-normalization group (RNG) model chosen as the turbulence closure. The collapsing rock mass was defined as a GMO and treated as a rigid body. Its motion within the flow field was captured using the FAVOR method. Based on the geological investigations and previous studies, the COR and the COF were set at 0.5 and 0.45, respectively[18,21-23]. The rock mass motion was specified using the coupled motion option. The fluid material was defined as water at 20 ℃.

For the boundary conditions, the lower boundary in the vertical (Z) direction was set as a wall, whereas the upper boundary was specified with a specific pressure. Both the fluid fraction and pressure at the top boundary were set to zero. Other boundaries retained their default settings. The established three-dimensional model for the impulse wave simulation is presented in Figure 4.

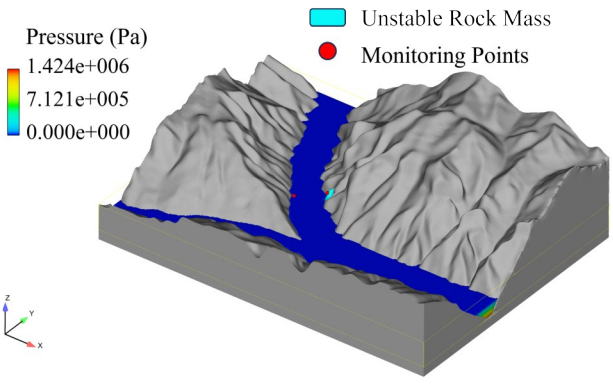

Fig. 4　Three-dimensional model for impulse wave simulation

In the model, the maximum water pressure is 1.424×10^6 Pa, whereas the free surface pressure is set to zero. The unstable rock mass is marked in blue. Monitoring points are indicated by red dots: Monitoring Point 1 is set on the unstable rock mass and moves with it, whereas Monitoring Point 2 is fixed on the opposite bank to record wave run-up height induced by the rock collapse.

3.3　Simulation Results

With the initial water level set at 162 m, the impulse waves triggered by cliff instability during the dry season were simulated. The generation, propagation, and run-up of the waves over 45 s are depicted in Figure 5.

As illustrated in Figure 5a, at t = 5.4 s, the unstable rock mass completely slid out from its foundation, exhibiting a pronounced toppling motion. The rock mass began to compress the water body, generating an initial impulse wave with an amplitude of approximately 7 m. At this stage, the rock mass was not yet fully submerged, and the continued compression of the water caused the wave to remain in its rising phase.

By t = 7.8 s, the rock mass became fully immersed in the water and its potential energy was fully converted (Figure 5b). At this moment, the impulse wave carried significant kinetic energy while its potential energy was relatively lower.

As shown in Figure 5c, at t = 8.4 s, the rock mass started to sink below the river surface. A pronounced upward jet was generated at the upper vertex of the submerged rock mass. The wave height on the upstream side was relatively higher, with the maximum amplitude having reached about 20 m.

At t = 9.5 s, the wave amplitude reached its peak of 27.4 m (Figure 5d). The location of the maximum wave height remained upstream of the collapse point. By this time, the wave had propagated to the opposite bank and initiated interaction with the shoreline. Prior to this interaction, the wave can be approximately characterized as a solitary wave; subsequently, its profile became considerably more complex.

As depicted in Figure 5e, at t = 10.2 s the wave reached a significant run-up height on the opposite bank. As the wave continued to propagate, its maximum amplitude began to decrease.

By t = 15.6 s, the wave further diffused both upstream and downstream, with a continued reduc-

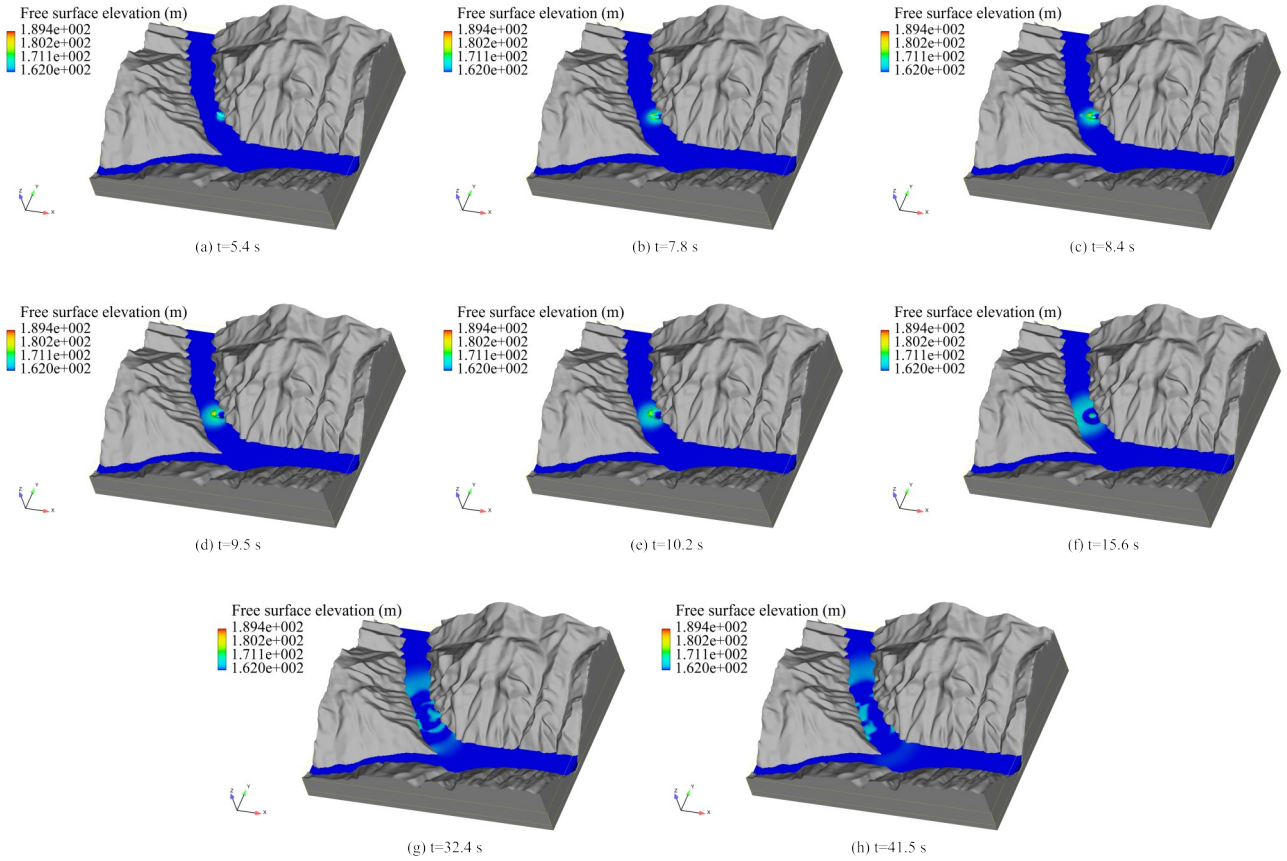

Fig. 5 Simulation results of impulse waves under the 162 m water level

tion in amplitude after impacting the opposite bank (Figure 5f). The wave dynamics subsequently grew more complex.

During the later complex wave interaction stages at t = 32.4 s and t = 41.5 s (Figures 5g and 5h, respectively), two notable run-up events were recorded on the bank opposite the collapse site. By this stage, the wave energy had gradually dissipated, with both flow velocity and wave height markedly reduced. These two higher run-up events were attributed to wave superposition. Thereafter, the impulse wave progressively dissipated.

The main findings of this study can be summarized as follows: (1) Under the 162 m water level, the simulated collapse generates an impulse wave with a maximum amplitude of 27.4 m, exhibiting a four-phase evolution process encompassing generation, propagation, run-up with complex shoreline interaction, and eventual dissipation. (2) The parameter sensitivity analysis reveals asymmetric and metric-specific influences: the COF dominantly controls the minimum free surface elevation (with a high relative sensitivity coefficient, RSC $\approx$ -1.27 for a -20% change), whereas the COR primarily governs the maximum velocity of the rock mass (RSC $\approx$ -0.52 for a -20% change). (3) In contrast, the maximum free surface elevation shows negligible sensitivity to $\pm 20\%$ variations in either parameter, indicating relative robustness in predicting the peak wave height under the given modeling setup.

4 Discussion

4.1 Characteristics of Impulse Waves under the 162 m Water Level

The simulated wave generation and propagation process can be divided into four distinct phases.

The wave generation phase (from initiation to approximately 7.8 s) was the critical period for initial energy input. The rock mass slid into the water in a toppling manner, continuously compressing the water ahead and transferring its potential and kinetic energy to the fluid, thereby exciting the initial impulse wave. During this phase, the wave height was in a state of continuous increase, and the rock mass was not yet fully submerged.

The subsequent propagation phase (approxi-

mately 7.8 s to 9.5 s) was characterized by energy transfer and significant waveform evolution. As the rock mass became fully submerged and the energy input ceased, the kinetic energy of the wave reached its peak. The wave height increased rapidly during propagation, reaching a maximum amplitude of 27.4 m, with a greater height observed on the upstream side. A pronounced upward jet was generated by the submerged rock motion. Prior to reaching the slope, the wave profile could be reasonably approximated as a solitary wave.

Upon reaching the opposite bank, the process entered the run-up and complex interaction phase (approximately 9.5 s to 41.5 s), the core of which involved intense wave-slope interaction and energy redistribution. Following the initial interaction with the slope, the wave profile grew significantly more complex and induced substantial run-up. Notably, subsequent reflections and wave superposition triggered two higher run-up events at around 32.4 s and 41.5 s (Figure 6), highlighting the dynamic complexity of wave interactions during this stage.

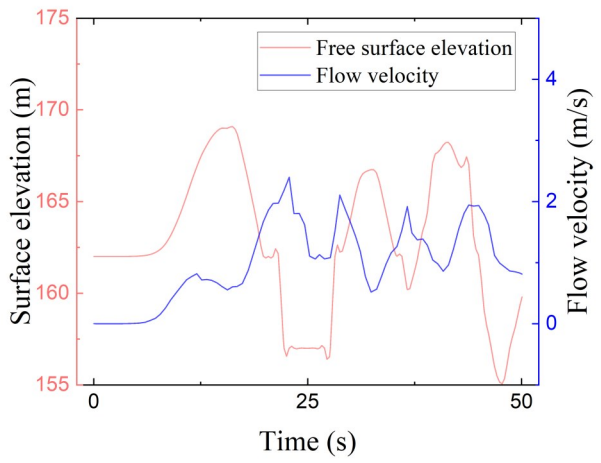

Fig. 6　Hydrodynamic characteristics at the opposite bank

Finally, the system entered the dissipation phase after 41.5 s. After multiple reflections, superpositions, and run-up events, the wave energy was substantially consumed through mechanisms such as viscous dissipation and bottom friction. This was manifested by a marked attenuation in flow velocity and wave height, leading to the gradual subsidence of the initial impulsive wave motion.

4.2　OAT Sensitivity Analysis of the Wave Model

When using the GMO method to simulate the motion of an unstable rock mass after failure, the COR and COF are key parameters governing the movement characteristics. The COR controls the energy loss during collisions between the rock mass and the reservoir bank, whereas the COF governs the magnitude of friction between them. Due to the complex geological environment of the reservoir bank, direct experimental measurement of these parameters is often challenging. Common practice involves assigning values based on engineering experience, thus these parameters are subjected to significant uncertainty. Conducting an uncertainty analysis on these parameters, specifically investigating their influence on the maximum wave height, minimum wave height, and maximum rock mass velocity, helps quantify model uncertainty and assess the reasonableness of the parameter values chosen.

For the analysis, the COR and COF were each increased (or decreased) by 20% relative to their baseline values, and additional wave simulations were performed to examine changes in the model outputs.

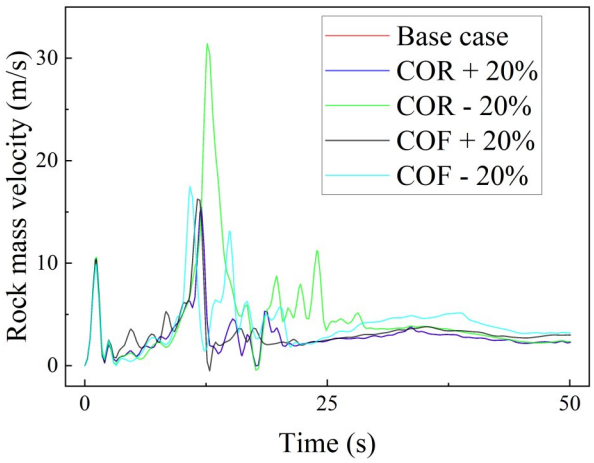

Fig. 7　Rock mass velocity time series under different COR and COF scenarios

The rock mass velocities recorded are shown in Figure 7. Within the first 2 s after instability, the rock mass velocities showed no significant differences. During this period, the rock mass slid out from its foundation, accelerated to approximately 10 m/s, and then collided with the reservoir bank, undergoing a brief deceleration phase. Subsequently, the rock mass began to topple and accelerate significantly. Distinct differences in velocity emerged during this stage, particularly when the COR was reduced, as the rock mass achieved a markedly higher maximum

velocity. In other simulation cases, the maximum velocities did not differ substantially. After reaching peak velocity, the rock mass gradually decelerated due to sustained friction and collisions with the bank until its motion essentially ceased.

The effects of the COR and COF on the maximum free surface elevation, minimum free surface elevation, and maximum rock mass velocity were quantified using the methodology described in Section 2.3. The results are presented in Table 1.

Based on the single-variable parameter sensitivity analysis, this study reveals that the influence of the COR and COF on different model output metrics differs significantly. Overall, the sensitivity exhibits pronounced asymmetry and imbalance.

The analysis indicates that the COF is the most critical parameter governing the minimum free surface elevation, and its influence shows strong directionality. When the COF decreased by 20%, the minimum elevation rises sharply from the baseline value of 83.54 m to 104.69 m. The corresponding RSC reaches －1.265, which falls within the highly sensitive range. In contrast, while the COR has a positive correlation with the minimum elevation, its sensitivity (RSC, 0.122) is significantly weaker than that of the COF.

Regarding the maximum rock mass velocity, the COR emerges as the dominant controlling parameter, particularly when its value is reduced. A 20% decrease in the COR causes the maximum velocity to surge from 15.46 m/s to 31.42 m/s, with RSC －0.516, indicating moderate to high sensitivity. This suggests that a lower restitution coefficient significantly increases the kinetic energy of the rock mass movement, directly affecting the assessment of disaster impact intensity. In contrast, variations in the COF have a relatively limited effect on the movement velocity ($|RSC| < 0.07$), implying that the friction coefficient plays a weaker role in regulating the motion energy in this model.

Table 1 Sensitivity of key output metrics to ± 20% variations in COR and COF

Parameter	Variation Direction	Max. Free Surface Elevation (m)	Min. Free Surface Elevation (m)	Max. Rock Mass Velocity (m/s)
Base Case		189.36	83.54	15.46
COR	Increase +20%	189.35 ($\Delta y = -0.01$, RSC ≈ −0.000 3)	83.54 ($\Delta y = 0.00$, RSC = 0.000 0)	15.46 ($\Delta y = 0.00$, RSC = 0.000 0)
	Decrease −20%	189.09 ($\Delta y = -0.27$, RSC ≈0.007 1)	79.46($\Delta y = -4.08$, RSC ≈0.122 2)	31.42 ($\Delta y = 15.96$, RSC ≈ −0.516 2)
COF	Increase +20%	188.94 ($\Delta y = -0.42$, RSC ≈0.011 1)	94.02 ($\Delta y = 10.48$, RSC ≈ −0.313 7)	14.18($\Delta y = -1.28$, RSC ≈0.041 4)
	Decrease −20%	189.62($\Delta y = 0.26$, RSC ≈ −0.006 9)	104.69 ($\Delta y = 21.15$, RSC ≈ −1.265 3)	17.49 ($\Delta y = 2.03$, RSC ≈ −0.065 6)

Note: Δy represents the amplitude of variation; RSC refers to the relative sensitivity coefficient.

It is noteworthy that the maximum free surface elevation is extremely insensitive to variations of ± 20% in both parameters (all |RSC| values < 0.012), with the maximum change being less than 0.5 m. This phenomenon indicates that the predicted peak of the catastrophic process remains relatively stable despite parameter variations.

The parameter influences exhibit clear asymmetry: for sensitive metrics, the impact of a parameter change in one direction (e.g., a decrease in COF or COR) is far greater than the impact of a change in the opposite direction. These analytical results clearly indicate that to enhance the reliability of model predictions, priority should be given to the precise calibration of the COF, which dominantly affects the prediction of the minimum free surface elevation, and the COR, especially within its lower range, which is crucial for predicting the maximum rock mass velocity.

The pronounced asymmetric sensitivities observed above can be fundamentally explained through the lens of energy conversion and fluid-solid momentum transfer. During the instability process, the initial gravitational potential energy of the rock mass is partitioned into frictional dissipation along the sliding/toppling path, the kinetic energy of the moving mass, and collision energy loss. The COF acts as a primary energy valve, directly governing the magnitude of the frictional work. A variation in the

COF significantly alters the remaining kinetic energy of the rock mass at the exact moment of water entry. From a hydrodynamic perspective, the formation of the wave trough (minimum free surface elevation) is macroscopically represented by the temporary plunge cavity created when the rock mass rapidly displaces the water body. The volume and depth of this cavity are strictly dependent on the intrusion momentum and impact kinetic energy of the landslide mass. Therefore, changes in the COF lead to non-linear variations in the impact kinetic energy, which in turn, drastically reshapes the fluid displacement cavity and dictates the extreme trough level of the impulse wave. Conversely, the COR primarily controls the degree of energy conservation during discrete rigid-body collisions (e. g., bouncing against the riverbed or the opposite bank). A lower COR restricts collision-induced rebounding and energy dissipation in the normal direction, causing the rock mass to convert more of its potential energy into translational sliding along the bed. This retained momentum dominantly drives the surge in the maximum recorded rock mass velocity, while having a relatively secondary effect on the initial fluid cavity formation.

5 Conclusion

This study conducted a numerical investigation of the impulse waves generated through the potential collapse of the Jianchuandong rocky cliff in the TGR area, using the FLOW-3D software with a fluid-solid coupling approach.

Compared with prior studies focusing predominantly on extreme water levels (145 m and 175 m), this study fills a knowledge gap by characterizing wave hazards under a representative operational level, thereby refining risk assessment across the entire reservoir scheduling cycle. Furthermore, by systematically quantifying parameter sensitivities, our findings challenge the common deterministic approach of assigning fixed empirical values to COR and COF. They underscore that parameter uncertainty, especially in the lower ranges of COF and COR, can significantly perturb predictions of key hazard indicators such as wave trough elevation and rock mass kinetic energy.

The underlying mechanisms for the observed asymmetric sensitivities may be related to the distinct roles of friction and restitution in different stages of energy conversion. We speculate that the COF strongly affects the initial sliding acceleration and the subsequent sustained friction during toppling, thereby heavily affecting the energy input into the water and the resulting wave trough. Conversely, the COR, by governing collision energy loss, becomes critical in determining the peak kinetic energy of the rock mass during impact and tumbling, which directly translates into the intensity of the fluid excitation.

The theoretical significance of this study relies in advancing the understanding of impulse wave generation under realistic, non-extreme reservoir conditions and in highlighting the importance of parameter uncertainty quantification in geohazard modeling. Practically, the results provide a more nuanced scientific basis for hazard assessment and risk management in the TGR area. The identified parameter sensitivities can guide the prioritization of field investigations and the calibration of numerical models for early warning systems.

Despite these contributions, this study has limitations. The sensitivity analysis adopted an OAT approach, which does not account for potential interactions between parameters. Furthermore, the geological and kinematic parameters were simplified; the rock mass was modeled as a rigid body with uniform properties, which may not fully capture the internal deformation and fragmentation during collapse.

To overcome these limitations, future research will focus on two main aspects: (1) using global sensitivity analysis coupled with probabilistic frameworks to decipher complex multi-parameter interactions, and (2) integrating advanced numerical methods (e. g., finite-discrete element method or coupled DEM-CFD) to capture the progressive fragmentation and granular flow characteristics of the collapsing rock mass. These targeted advancements will further refine the reliability of lifecycle risk management for reservoir geohazards.

References

[1] Liu Y H, Tu G X, Luo B, et al. Prediction of impulse

waves generated by the potential failure of large deposits in the Rumei Reservoir, Lancang River, China[J]. Canadian Geotechnical Journal, 2025, 62: 1-17.

[2] Zhang Y, Li D Y, Chen L X, et al. Numerical analysis of landslide-generated impulse waves affected by the reservoir geometry[J]. Engineering Geology, 2020, 266: 105390.

[3] Huang B L, Yin Y P, Tan J M. Risk assessment for landslide-induced impulse waves in the Three Gorges Reservoir, China[J]. Landslides, 2019, 16(3): 585-596.

[4] Huang B L, Wang S C, Zhao Y B. Impulse waves in reservoirs generated by landslides into shallow water[J]. Coastal Engineering, 2017, 123: 52-61.

[5] Dong X C, Huang B L, Li Q W, et al. Prediction of impulse waves generated by partially submerged landslides with a low Froude number based on prototype physical experiments[J]. Physics of Fluids, 2024, 36(10): 106630.

[6] Karahan M, Ersoy H, Akgun A. A 3D numerical simulation-based methodology for assessment of landslide-generated impulse waves: a case study of the Tersun Dam reservoir (NE Turkey)[J]. Landslides, 2020, 17(12): 2777-2794.

[7] Noda E. Water waves generated by landslides[J]. Journal of the Waterways, Harbors and Coastal Engineering Division, 1970, 96(4): 835-855.

[8] Fritz H M, Hager W H, Minor H E. Near field characteristics of landslide generated impulse waves[J]. Journal of Waterway, Port, Coastal, and Ocean Engineering, 2004, 130(6): 287-302.

[9] Zhao T, Utili S, Crosta G B. Rockslide and impulse wave modelling in the Vajont Reservoir by DEM-CFD analyses[J]. Rock Mechanics and Rock Engineering, 2016, 49(6): 2437-2456.

[10] Dutykh D, Katsaounis T, Mitsotakis D. Finite volume schemes for dispersive wave propagation and runup[J]. Journal of Computational Physics, 2011, 230(8): 3035-3061.

[11] Mahallem A, Roudane M, Krimi A, et al. Smoothed Particle Hydrodynamics for modelling landslide-water interaction problems[J]. Landslides, 2022, 19(5): 1249-1263.

[12] Vacondio R, Mignosa P, Pagani S. 3D SPH numerical simulation of the wave generated by the Vajont rockslide [J]. Advances in Water Resources, 2013, 59: 146-156.

[13] Ataie-Ashtiani B, Shobeyri G. Numerical simulation of landslide impulsive waves by incompressible smoothed particle hydrodynamics[J]. International Journal for Numerical Methods in Fluids, 2008, 56(2): 209-232.

[14] Yin Y P, Huang B L, Liu G N, et al. Potential risk analysis on a Jianchuandong dangerous rockmass-generated impulse wave in the Three Gorges Reservoir, China[J]. Environmental Earth Sciences, 2015, 74(3): 2595-2607.

[15] Wang L Q, Yin Y P, Huang B L, et al. Damage evolution and stability analysis of the Jianchuandong Dangerous Rock Mass in the Three Gorges Reservoir Area[J]. Engineering Geology, 2020, 265: 105439.

[16] Huang J, Li J Q, Liang P T. Inflow flood simulation and risk analysis of cascade reservoirs[J]. MATEC Web of Conferences, 2018, 246: 01106.

[17] Snelling B, Neethling S, Horsburgh K, et al. Uncertainty quantification of landslide generated waves using Gaussian process emulation and variance-based sensitivity analysis[J]. Water, 2020, 12(2): 416.

[18] Sabeti R, Heidarzadeh M. Numerical simulations of tsunami wave generation by submarine landslides: validation and sensitivity analysis to landslide parameters [J]. Journal of Waterway, Port, Coastal, and Ocean Engineering, 2022, 148(2): 05021016.

[19] Hirt C W. Volume-fraction techniques: powerful tools for wind engineering[C]//Proceedings of the 1st International Symposium on Computational Wind Engineering (CWE 92), Tokyo, Japan, August 21-23, 1992: 327-338.

[20] Yin Y P, Wang L Q, Zhang W G, et al. Research on the collapse process of a thick-layer dangerous rock on the reservoir bank[J]. Bulletin of Engineering Geology and the Environment, 2022, 81(3): 109.

[21] Franco A, Moernaut J, Schneider-Muntau B, et al. Triggers and consequences of landslide-induced impulse waves-3D dynamic reconstruction of the Taan Fiord 2015 tsunami event[J]. Engineering Geology, 2021, 294: 106384.

[22] Chen S Z, Shi A C, Xu W Y, et al. Numerical investigation of landslide-induced waves: a case study of Wangjiashan landslide in Baihetan Reservoir, China[J]. Bulletin of Engineering Geology and the Environment, 2023, 82(4): 110.

[23] Yin B G, Yin Y P, Zhang Z H, et al. Geostructures, dynamics and risk assessment on rockfall fragmentation flow at the Wuxia Gorge, the Three Gorges Reservoir, China[J]. Bulletin of Engineering Geology and the Environment, 2025, 84(7): 368.

(编辑 XXX)